Supplementary Materials for

Substorm-like aurora at Jupiter

B. Bonfond[1]*†, Z. H. Yao[1,2]†, G. R. Gladstone[3], D. Grodent[1], J.-C. Gérard[1], J. Matar[1], T. K. Greathouse[3], V. Hue[3], M. H. Versteeg[3], J. A. Kammer[3], C. Tao[4], M. Vogt[5], A. Mura[6], A. Adriani[6], B. Mauk[7], W. Kurth[8], S. Bolton[3]

Correspondence to: b.bonfond@uliege.be

This PDF file includes:

Materials and Methods

Juno-UVS is an imaging spectrograph operating in the 68 to 210 nm range (*5,32*). Its dog-bone shaped slit is 7.2° long, 0.025° wide in the center and 0.2° wide in the two extremities. The slit is generally oriented perpendicularly to the spin axis. However, a scan mirror located at the entrance of the instrument allows the field of view to shift by up to +/-30° from the spin plane. In the present work, only the data from the wide parts of the slit are used, in order to optimize the signal to noise ratio. Moreover, the wavelength range from 155 to 162 nm is selected in order to avoid regions affected by absorption of the UV light by hydrocarbon molecules in the Jovian atmosphere (mostly methane).

The calibrated data from Juno-UVS are available through the Planetary Data System in the form of .FITS files, which contain information about each event collected by the detector, such as the time of the event, its position in X and Y on the detector, the corresponding wavelength, etc. This first step of the processing consists of removing the noise due to particle (typically relativistic electrons) penetrating into the instrument and impacting the detector from the signal caused by UV photons. Contrary to photons, which are diffracted by the grating, penetrating particles illuminate the detector in an almost homogenous fashion, as confirmed by observations carried out in the radiation belts. We use a region between pixels 345 to 550 in the X direction (corresponding to ~59.7 to 80.9 nm) and pixels 20 to 255 in the Y direction, which has a very low effective area for extreme-UV photons (*33*), in order to estimate the count rate per pixel due to radiation. This background noise is then removed from the photon illuminated part of the detector.

The second step consists, for each detection event, in projecting the four corners of each field of view element along the slit onto a Jupiter-shaped ellipsoid located 400 km above the 1 bar level, using the SPICE kernels listed in the .FITS file header. The brightness, which is derived from the weighted counts and the exposure time, is then attributed to quadrilateral formed by these 4 points. A map of the aurora is then progressively built by adding all the detection events for a given Juno spin. Simultaneously, an exposure map, identifying the regions of the planet covered by the instrument's field of view, is also built. Images of the whole aurorae are then assembled by performing a weighted sum of the consecutive spins, with a higher weight being attributed to the latest spin. We then divide the weighted sum of the counts with a weighted sum of the exposure maps to derive our final brightness map. This method offers the best compromise between the completeness of the auroral map and the dynamics of the auroral features.

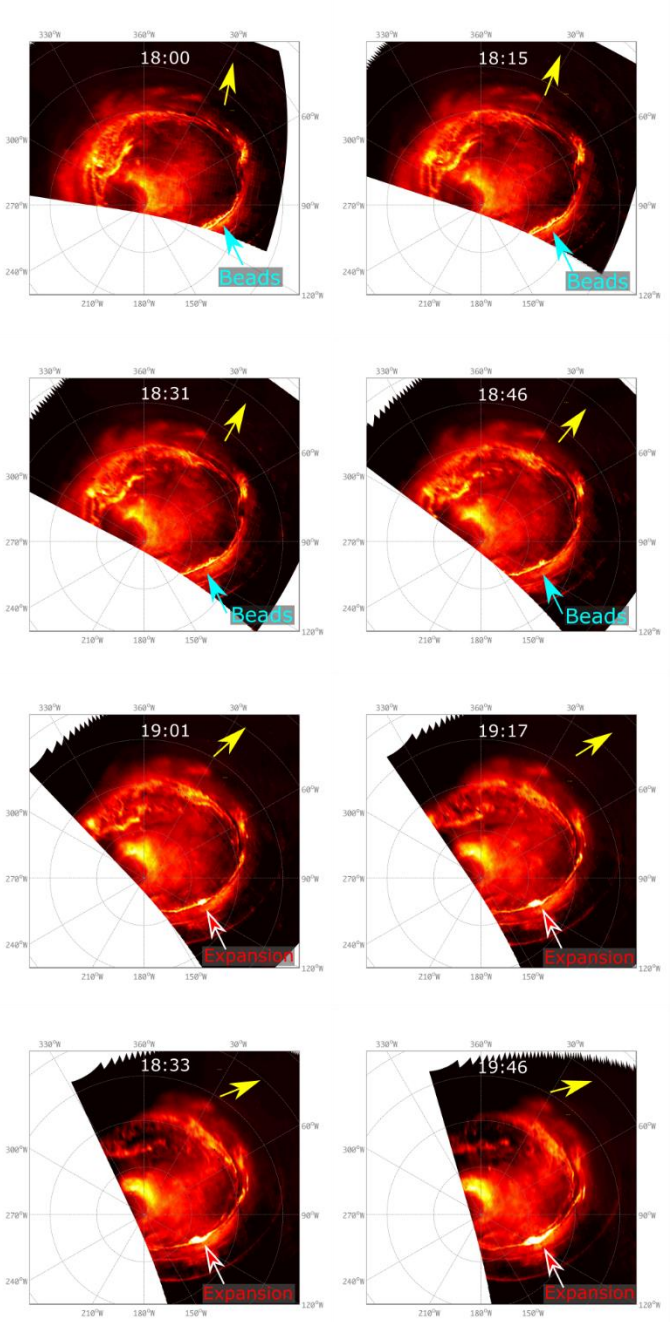

Fig. S1.

Polar projections of the southern aurorae observed by the JIRAM infrared instrument (*31*) after the last Juno-UVS observations of the first perijove (PJ1)(34). During this sequence, the post-midnight/dawn part of the main emission becomes irregular. The main emission then strongly brightens and this bright section expands both in longitude and latitude. These might correspond to the onset and beginning of the expansion of a dawn storm.

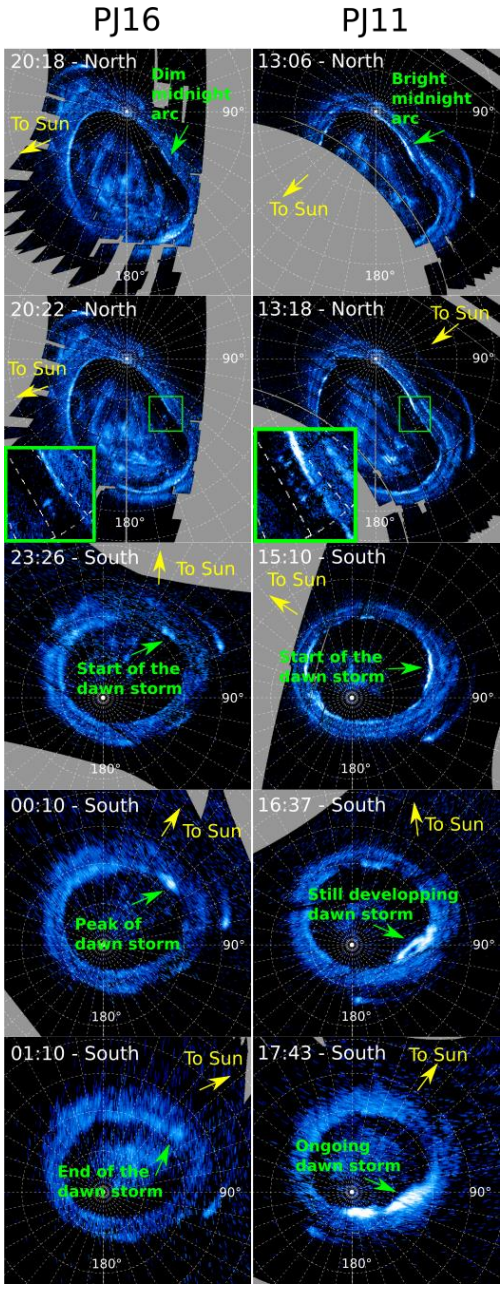

Fig. S2.

The left column shows polar projections of the aurorae during the 16th perijove, and the right column shows a similar sequence for the 11th perijove. While the sequence on PJ11 compares with a terrestrial substorm (Fig. 1-2), the one on PJ16 is much more limited in size, emitted power and duration and would be more similar to a terrestrial pseudo-breakup.

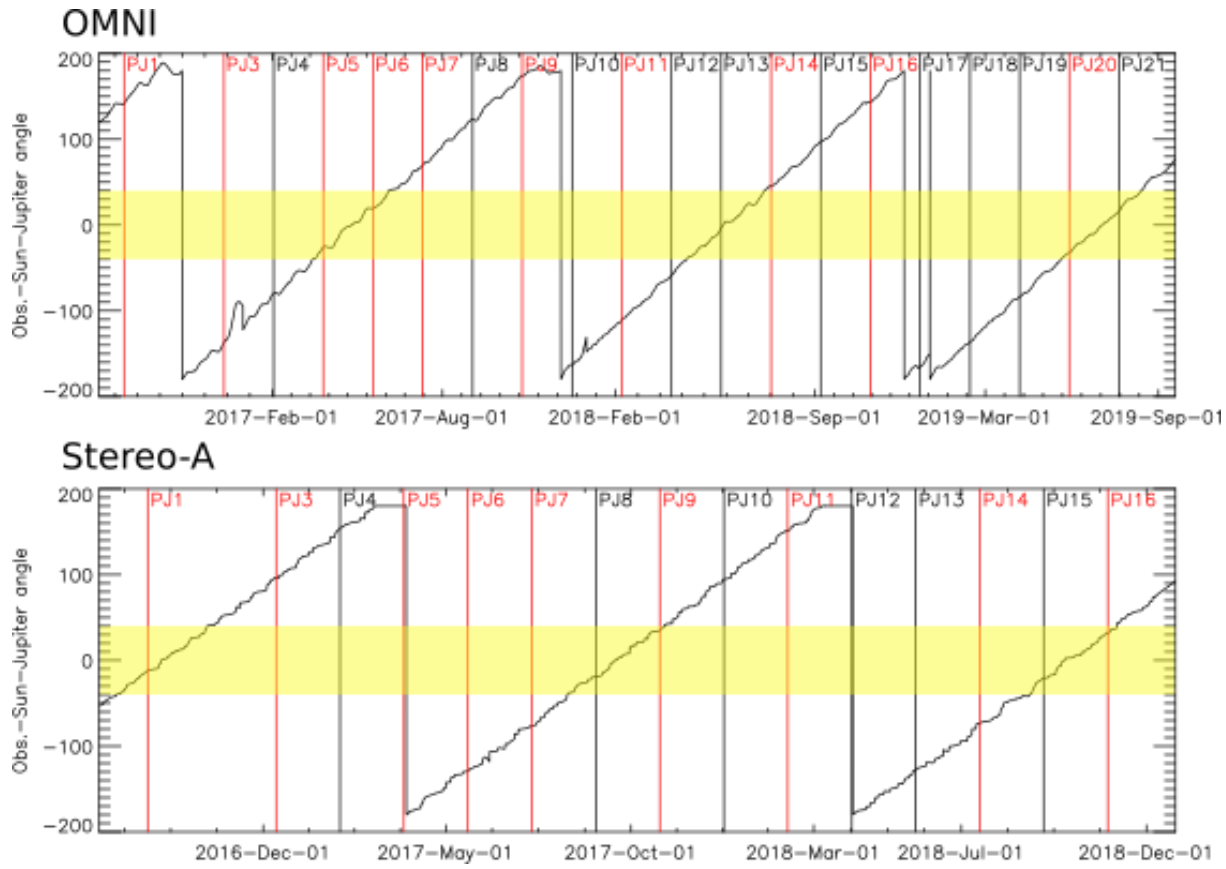

Fig. S3.

Angle between the Earth-based solar wind observatories (top) or Stereo-A (bottom) and Jupiter as seen from the Sun. The yellow regions highlight the time intervals during which Jupiter was less than 40° away from the solar wind observatories under consideration. The vertical lines correspond to the perijove times and those in red correspond to the one during which dawn storms were identified.

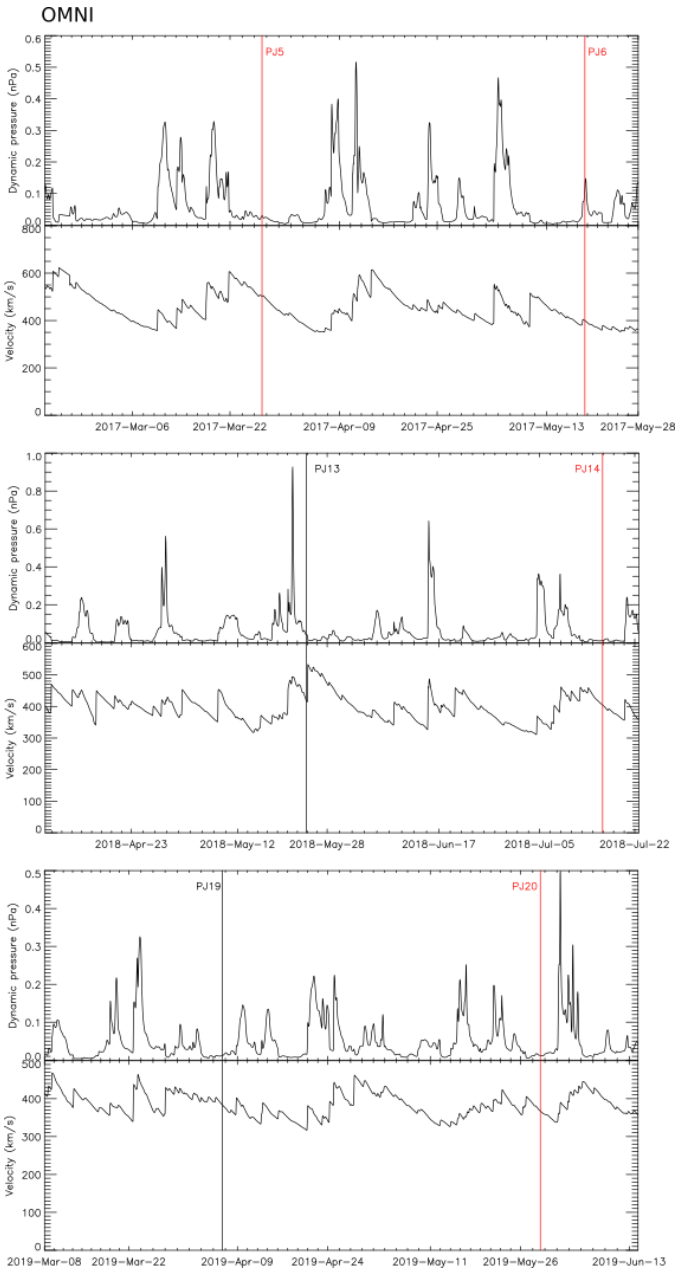

Fig. S4.

Outputs of the Tao et al. model(*6*)(22) extrapolating the solar wind properties to Jupiter's distance based on measurements from Earth-bound satellites (obtained from the AMDA website http://amda.irap.omp.eu/) for the three time intervals during which the Earth and Jupiter were aligned within 40°. The vertical lines show the times of the perijoves during these intervals and the red line identify perijoves during which a dawn storm was observed. For each interval, the top plot shows the dynamic pressure and the bottom plot shows the radial velocity. It can be seen that the solar wind was quiet during PJ5, PJ14 and PJ20, even if we account for a timing uncertainty of 1-2 days. PJ6 may have been concurrent with a limited solar wind enhancement.

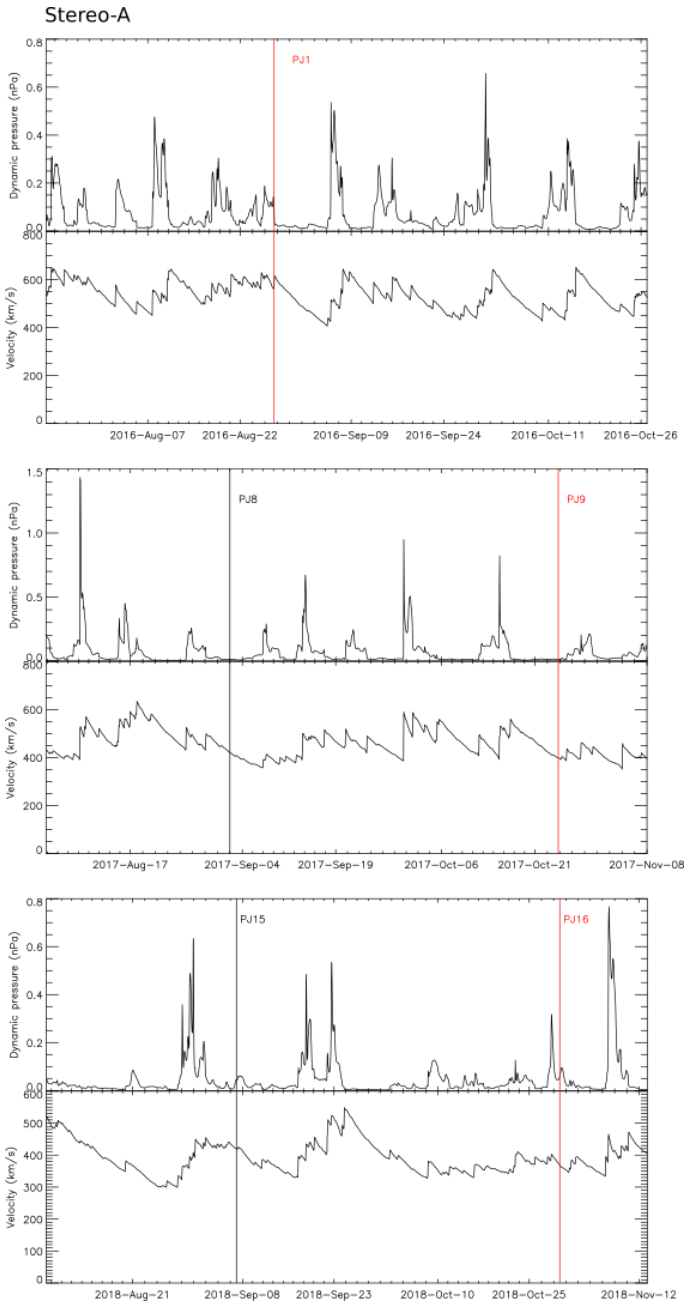

Fig. S5.

Same as for figure S3, but based on Stereo A solar wind measurement instead of measurements from Earth-based satellites. The solar wind was quiet during the dawn storm observed on PJ9. Acknowledging a 1-2 days propagation uncertainty, PJ1 and PJ16 may have been concurrent with some solar wind enhancements.